

Scattering Attenuation of 2D Elastic Waves: Theory and Numerical Modeling Using a Wavelet-Based Method

by Tae-Kyung Hong and B. L. N. Kennett

Abstract The passage of seismic waves through highly heterogeneous media leads to significant scattering of seismic energy and an apparent attenuation of seismic signals emerging from the heterogeneous zone. The size of this scattering attenuation depends on the correlation properties of the medium, the rates of P- and S-wave velocities, and frequency content of the incident waves. An estimate of the effect can be obtained using single scattering theory (first-order Born approximation) for path deviations beyond a minimum scattering angle; smaller deviations require consideration of multiple scattering or a representation in terms of travel-time perturbations. Although an acoustic treatment provides a quantitative reference, full elastic effects need to be taken into consideration to get an accurate attenuation rates. The use of a wavelet-based modeling technique, which is accurate and stable even in highly perturbed media, allows an assessment of the properties of different classes of stochastic media (Gaussian, exponential, von Karman). The minimum scattering angle for these stochastic media is in the range of 60° to 90° . The wavelet-based method provides a good representation of the scattered coda, and it appears that methods such as finite differences may overestimate scattering attenuation when the level of the heterogeneity is high.

Introduction

One of the most important topics in regional seismic studies is the influence of scattering due to material inhomogeneities and anisotropy in the crust and the upper mantle (Nolet *et al.*, 1994, Wu *et al.*, 1994). Scattering processes modify both the travel times and amplitudes of seismic waves. A full representation of scattering phenomena requires consideration of multiple scattering effects, which are difficult to handle. In consequence, attention has focused on single scattering implemented via a first-order Born approximation for weakly heterogeneous regions (Wu, 1982; Frankel and Clayton, 1986).

The single scattering theory is applied mainly to back-scattered and side-scattered energy, and the more complex effects in forward scattering are taken care of by including a correction for the induced travel-time shift inside a certain angular range around the propagation direction. The separation between the two different approximation regimes is made at the “minimum (or, cutoff) scattering angle” (Roth and Korn, 1993; Sato and Fehler, 1998; Kawahara, 2002). Estimates of this minimum scattering angle have been made using numerical modeling of stochastic media in an acoustic approximation or with a full elastic treatment (Frankel and Clayton, 1986; Jannaud *et al.*, 1991; Roth and Korn, 1993; Frenje and Juhlin, 2000). Alternatively, estimates of the minimum scattering angle have been made theoretically for random acoustic media (Sato, 1984; Kawahara, 2002).

However, there is still some uncertainty as to the appropriate minimum scattering angle for elastic waves because much of the work has been undertaken in the acoustic approximation (Roth and Korn, 1993) or with a scalar wave approach, even for elastic wave studies (Frankel and Clayton, 1986). The scattering pattern of elastic waves is complex and is significantly different from that of scalar waves (Wu and Aki, 1985) due to the inherent characteristics of elastic waves such as wave-type coupling, the radiation patterns in scattering, and complex interferences between the waves. As a result, numerical modeling for elastic waves needs to be compared with theoretical results for a full understanding of the influence of elastic wave scattering. The minimum scattering angle, as one of the key factors in single scattering theory, thus needs to be determined properly and the relation to the acoustic theory explored.

Single scattering theory for 3D elastic waves has been developed in several studies. Wu and Aki (1985) compared theoretical scattering coefficients based on the Born approximation with results derived from observations and tried to reveal the characteristics of heterogeneities in the lithosphere. Wu (1989) introduced the “perturbation method” for the scattering of elastic waves in random media, which considers the scattering waves as the response of the perturbations to the incident waves in a sense of a radiation problem.

Sato and Fehler (1998) followed a similar approach but considered an additional important factor, a travel-time correction applied to the Born approximation, to determine the correct energy loss during scattering. They associated the travel-time shift by the fractional-velocity fluctuation due to the long wavelength component of scattered waves, that is, waves with wavelength more than twice that of the dominant frequency. This approach has been used to determine the minimum scattering angle to be employed in the estimation of scattering attenuation of elastic waves in 3D.

It is therefore important to check that the theoretical estimates of the minimum scattering angle match those determined empirically. Although Sato and Fehler's minimum scattering angle is supported by some numerical studies (Roth and Korn, 1993) for the scalar-wave cases, it has not been fully checked for elastic waves. The numerical studies of elastic waves (Frankel and Clayton, 1986) used the theoretical attenuation curve for scalar waves as the reference curve for determining the minimum scattering angle. However, since numerical modeling for 3D elastic wave propagation still requires considerable computational expense to achieve an adequate domain for the assessment of the scattered energy, we confine our study to 2D elastic waves.

For 2D elastic waves, hybrid methods have been used. Fang and Müller (1996) attempted to formulate the governing equation in a rational form by incorporating two formulae for scalar waves with both velocity perturbation (Frankel and Clayton, 1986) and density perturbation (Roth and Korn, 1993). The coefficients of each term in the rational form need to be determined for each stochastic medium by curve fitting to the results from numerical experiments. This approach of Fang and Müller is based on the fundamental assumption that the scattering attenuation pattern of elastic waves is similar to that of scalar waves for the given stochastic medium (e.g., exponential media for Fang and Müller's study) and that the minimum scattering angle (θ_{\min}) would be the same (20°) for both acoustic and elastic waves.

To avoid such assumptions, it is important to develop a fully elastic 2D theory for the variation of scattering attenuation as a function of normalized wavenumber for 2D elastic waves to compare with numerical results, and thereby determine the minimum scattering angle.

It is very important that we have not only a correct derivation and implementation of scattering theory for comparisons with numerical results, but also that high-accuracy numerical modeling is available for assessing the value of the minimum scattering angle. The finite difference method (FDM) with fourth-order accuracy in spatial differentiation has been used widely for modeling in random heterogeneous media due to the convenience in treatment of numerical models and simplicity in implementation (Frankel and Clayton, 1986; Jannaud *et al.*, 1991; Roth and Korn, 1993; Fang and Müller, 1996; Frenje and Juhlin, 2000; Fehler *et al.*, 2000). However, Sato and Fehler (1998) have pointed out that derivatives in a FDM scheme are computed in the sense of an average over some grid points in a domain. Therefore,

it is still an open question as to whether the fourth-order accuracy in spatial differentiation is sufficient for stable and accurate modeling in random heterogeneous media.

High accuracy in spatial differentiation can be achieved with the pseudospectral method, and this approach has been applied in seismic wavefield computation for laterally heterogeneous models on upper mantle and global scales (Furumura *et al.*, 1999). However, it is difficult to achieve a comparable level of accuracy in the representation of the free-surface condition of vanishing traction. Yomogida and Benites (1995) have applied the boundary integral method for modeling media with randomly distributed cavities. Such boundary integral methods can deal well with heterogeneities inside a medium with irregular interfaces (e.g., cavities, cracks). The boundary conditions are satisfied by including effective sources at the boundaries at each time step. For a homogeneous medium, it is possible to get an accurate time response because the necessary Green's functions can be found analytically. However, it is difficult for the method to be applied to media with heterogeneous backgrounds (including layered media) because the Green's functions themselves need to be found numerically. Recently, the generalized screen propagators (GSP) method has been developed as a fast computational procedure for modeling of elastic wave propagation in half spaces with small-scale heterogeneities (Wu *et al.*, 2000). However, the approach used in the GSP method ignores the backscattering process and so is not suitable for full representation of scattered waves.

In this study, we use a wavelet-based method (WBM; Hong and Kennett, 2002a,b) as an accurate and stable simulator of elastic wave propagation in random media. The accuracy and the stability of the method is addressed by comparisons with the FDM. The WBM is then applied to calculate synthetic seismograms for several styles of stochastic media, from which the scattering attenuation is measured. The nature of the scattering needs to be taken into account to get accurate estimates of the attenuation, since in large-scale heterogeneity, significant deviations in the primary wave field mean that both components of motion need to be considered for a 2D medium. With accurate modeling we are able to place constraints on the minimum scattering angle for 2D elastic waves to the span of 60° – 90° .

Derivation of Q_s^{-1} from Single Scattering Theory

We estimate the scattering attenuation factors (Q_s^{-1}) as a function of normalized wavenumber (ka) based on single scattering theory in 2D random heterogeneous media, where k is the wavenumber of incident waves and a is the correlation distance.

We represent the wavefield (u_j , $j = x, z$) as composed of primary waves (u_j^0 , $j = x, z$) and scattered waves (u_j^s , $j = x, z$). The primary waves in 2D elastic media satisfy the relationships

$$\rho_0 \frac{\partial^2 u_x^0}{\partial t^2} = \frac{\partial \sigma_{xx}^0}{\partial x} + \frac{\partial \sigma_{xz}^0}{\partial z}, \quad \rho_0 \frac{\partial^2 u_z^0}{\partial t^2} = \frac{\partial \sigma_{xz}^0}{\partial x} + \frac{\partial \sigma_{zz}^0}{\partial z}, \quad (1)$$

where

$$\begin{aligned} \sigma_{xx}^0 &= (\lambda_0 + 2\mu_0) \frac{\partial u_x^0}{\partial x} + \lambda_0 \frac{\partial u_z^0}{\partial z}, \\ \sigma_{zz}^0 &= \lambda_0 \frac{\partial u_x^0}{\partial x} + (\lambda_0 + 2\mu_0) \frac{\partial u_z^0}{\partial z}, \\ \sigma_{xz}^0 &= \mu_0 \left(\frac{\partial u_x^0}{\partial z} + \frac{\partial u_z^0}{\partial x} \right), \end{aligned} \quad (2)$$

λ_0 and μ_0 are Lamé coefficients, and ρ_0 is the density in the background medium. When vertically incident (z -axis direction) plane P waves (Fig. 1) are considered as the primary waves, they are represented as

$$u_x^0 = 0, \quad u_z^0 = e^{i(k_\alpha z - \omega t)}, \quad (3)$$

where ω is the angular frequency, k_α is the wavenumber of incident P waves (ω/α_0), and α_0 is the background P velocity. The scattered waves can be represented using body forces f_j^s ($j = x, z$ or 1, 2) arising from the scattering effects of the variation of physical parameters,

$$\begin{aligned} \rho_0 \frac{\partial^2 u_x^s}{\partial t^2} - \frac{\partial \sigma_{xx}^s}{\partial x} - \frac{\partial \sigma_{xz}^s}{\partial z} &= f_x^s, \\ \rho_0 \frac{\partial^2 u_z^s}{\partial t^2} - \frac{\partial \sigma_{xz}^s}{\partial x} - \frac{\partial \sigma_{zz}^s}{\partial z} &= f_z^s. \end{aligned} \quad (4)$$

The body forces f_j^s in equation (4) can be found from the primary waves and the fluctuation of physical parameters as (cf. Sato and Fehler, 1998, equation 4.35)

$$f_x^s = -ik_\alpha \frac{\partial}{\partial x} (\delta\lambda) u_z^0, \quad f_z^s = - \left\{ k_\alpha^2 (\alpha_0^2 \delta\rho - \delta\lambda - 2\delta\mu) + ik_\alpha \frac{\partial}{\partial z} (\delta\lambda + 2\delta\mu) \right\} u_z^0. \quad (5)$$

From empirical studies (Birch, 1961, Shiomi *et al.*, 1996) on the perturbations of elastic wave velocities and mass density in real media that display a linear relationship among the parameters, we can represent the perturbations concisely in general by introducing a fractional-fluctuation term $\xi(x, z)$ as (Roth and Korn, 1993, Sato and Fehler, 1998, Section 4.2.2)

$$\xi(x, z) = \frac{\delta\alpha}{\alpha_0} = \frac{\delta\beta}{\beta_0} = \frac{1}{K} \frac{\delta\rho}{\rho_0} \quad (6)$$

where α_0 is the P -wave velocity in the background medium, β_0 is the S -wave velocity, and K is a constant that controls the magnitude of the density fluctuations. Hereafter we use

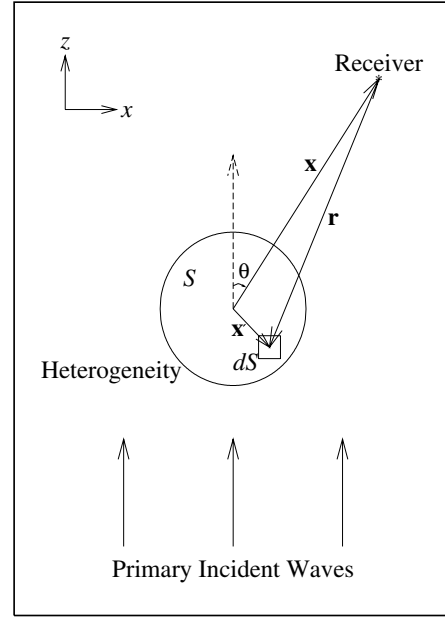


Figure 1. The scattering of the primary incident waves at the scatterer dS , a part of the whole heterogeneous area S . θ is the scattering angle from the incident direction of primary waves along the z axis. \mathbf{x} , \mathbf{x}' are the location vectors for the receiver and a scatterer. r links the scatterer to the receiver.

symbols without the subscript 0 to represent the background medium to simplify the mathematical expressions. Equation (5) can be rewritten from equation (6) as

$$\begin{aligned} f_x^s &= -ik_\alpha \alpha^2 \rho C_1 \frac{\partial \xi}{\partial x} \exp [i(k_\alpha z - \omega t)], \\ f_z^s &= \left(2k_\alpha^2 \alpha^2 \rho \xi - ik_\alpha \alpha^2 \rho C_2 \frac{\partial \xi}{\partial z} \right) \exp [i(k_\alpha z - \omega t)], \end{aligned} \quad (7)$$

where C_1 and C_2 are constants given by

$$C_1 = (K + 2) \left(1 - \frac{2\beta^2}{\alpha^2} \right), \quad C_2 = K + 2. \quad (8)$$

The solution of u_j^s ($j = x, z$ or 1, 2) in equation (4) can be expressed using the Green's function in the frequency domain, $\bar{G}_{jk}(\mathbf{x}, \mathbf{x}')$ and body forces by an integral over the area of heterogeneity S as (Roth and Korn, 1993)

$$u_j^s(\mathbf{x}) = \sum_{k=1}^2 \int_S f_k^s(\mathbf{x}') \bar{G}_{jk}(\mathbf{x}, \mathbf{x}') dS(\mathbf{x}'), \quad j = 1, 2. \quad (9)$$

The Green's function (G_{jk} , $j, k = 1, 2$) for 2D elastic wave equations (1) for a vertically directed point force can be written as (Burridge, 1976, p. 115)

$$\begin{aligned} \begin{pmatrix} G_{12} \\ G_{22} \end{pmatrix} &= \frac{1}{4\pi\rho r^2} \begin{pmatrix} (2t^2 - r^2/\alpha^2) \sin\theta\cos\theta \\ t^2\cos^2\theta - (t^2 - r^2/\alpha^2) \sin^2\theta \end{pmatrix} \frac{H(t - r/\alpha)}{\sqrt{t^2 - r^2/\alpha^2}} \\ &+ \frac{1}{4\pi\rho r^2} \begin{pmatrix} (-2t^2 + r^2/\beta^2) \sin\theta \cos\theta \\ t^2 \sin^2\theta - (t^2 - r^2/\beta^2) \cos^2\theta \end{pmatrix} \frac{H(t - r/\beta)}{\sqrt{t^2 - r^2/\beta^2}}, \end{aligned} \tag{10}$$

where θ is the angle between vertical axis (z) and wave propagation direction and $H(t)$ is the Heaviside step function. In this case, the far-field P and S waves can be written simply as

$$\begin{pmatrix} G_{12}^P \\ G_{22}^P \end{pmatrix} = \frac{\cos\theta}{4\pi\alpha^2\rho} \begin{pmatrix} \sin\theta \\ \cos\theta \end{pmatrix} \frac{H(t - r/\alpha)}{\sqrt{t^2 - r^2/\alpha^2}}, \tag{11}$$

and

$$\begin{pmatrix} G_{12}^S \\ G_{22}^S \end{pmatrix} = \frac{\sin\theta}{4\pi\beta^2\rho} \begin{pmatrix} -\cos\theta \\ \sin\theta \end{pmatrix} \frac{H(t - r/\beta)}{\sqrt{t^2 - r^2/\beta^2}}. \tag{12}$$

We can replace $H(t - r/c)/\sqrt{t^2 - (r/c)^2}$ in equations (11) and (12) with the zeroth-order Hankel function of the first kind ($H_0^{(1)}$) by using the Fourier transform (F) as (cf., Aki and Richards, 1980, ch. 6; Kennett, 1983, ch. 7)

$$\mathcal{F}\left[\frac{H(t - r/c)}{\sqrt{t^2 - (r/c)^2}}\right] = i\pi H_0^{(1)}(\omega r/c), \tag{13}$$

where $t > r/c$, ω is angular frequency and c is a wave velocity. We introduce the wavenumbers of P and S waves as k_α and k_β and write r for $|\mathbf{x} - \mathbf{x}'|$ (Fig. 1), to simplify equations (11) and (12) to the form

$$\begin{pmatrix} \bar{G}_{12}^P \\ \bar{G}_{22}^P \end{pmatrix} = \frac{i\cos\theta}{4\alpha^2\rho} H_0^{(1)}(k_\alpha|\mathbf{x} - \mathbf{x}'|) \begin{pmatrix} \sin\theta \\ \cos\theta \end{pmatrix}, \tag{14}$$

and

$$\begin{pmatrix} \bar{G}_{12}^S \\ \bar{G}_{22}^S \end{pmatrix} = \frac{i\sin\theta}{4\beta^2\rho} H_0^{(1)}(k_\beta|\mathbf{x} - \mathbf{x}'|) \begin{pmatrix} -\cos\theta \\ \sin\theta \end{pmatrix}. \tag{15}$$

We assume that the receiver is far away from the scatterers (i.e., $|\mathbf{x}| \gg |\mathbf{x}'|$; e.g., Roth and Korn, 1993), and then we can use the asymptotic expansion of Hankel function (Arfken, 1985, p. 618) and approximate $1/|\mathbf{x} - \mathbf{x}'|$ by $1/|\mathbf{x}|$ and $|\mathbf{x} - \mathbf{x}'|$ by $|\mathbf{x}| - \mathbf{n}\cdot\mathbf{x}'$ where \mathbf{n} is the unit vector in x direction. The approximate Green's functions take the form

$$\begin{pmatrix} \bar{G}_{12}^P \\ \bar{G}_{22}^P \end{pmatrix} = \frac{i}{4\alpha^2\rho} \sqrt{\frac{2}{\pi k_\alpha|\mathbf{x}|}} \exp\left[i\left(k_\alpha|\mathbf{x}| - k_\alpha\mathbf{n}\cdot\mathbf{x}' - \frac{\pi}{4}\right)\right] \begin{pmatrix} \sin\theta\cos\theta \\ \cos^2\theta \end{pmatrix}, \tag{16}$$

and

$$\begin{pmatrix} \bar{G}_{12}^S \\ \bar{G}_{22}^S \end{pmatrix} = \frac{i}{4\beta^2\rho} \sqrt{\frac{2}{\pi k_\beta|\mathbf{x}|}} \exp\left[i\left(k_\beta|\mathbf{x}| - k_\beta\mathbf{n}\cdot\mathbf{x}' - \frac{\pi}{4}\right)\right] \begin{pmatrix} -\sin\theta\cos\theta \\ \sin^2\theta \end{pmatrix}, \tag{17}$$

The Green's functions for far-field P and S waves for a horizontally directed point force can be obtained in the same way. We can therefore make a compact representation of the far-field Green's functions as

$$\begin{aligned} \bar{G}_{jk}^P &= \frac{i}{4\alpha^2\rho} \sqrt{\frac{2}{\pi k_\alpha|\mathbf{x}|}} \exp\left[i\left(k_\alpha|\mathbf{x}| - k_\alpha\mathbf{n}\cdot\mathbf{x}' - \frac{\pi}{4}\right)\right] A_{jk}^P(\theta), \\ \bar{G}_{jk}^S &= \frac{i}{4\beta^2\rho} \sqrt{\frac{2}{\pi k_\beta|\mathbf{x}|}} \exp\left[i\left(k_\beta|\mathbf{x}| - k_\beta\mathbf{n}\cdot\mathbf{x}' - \frac{\pi}{4}\right)\right] A_{jk}^S(\theta), \end{aligned} \tag{18}$$

where $A_{jk}^P(\theta)$ and $A_{jk}^S(\theta)$ are given by

$$\begin{aligned} A_{11}^P(\theta) &= \sin^2\theta, & A_{12}^P(\theta) &= \sin\theta\cos\theta, \\ A_{21}^P(\theta) &= -\sin\theta\cos\theta, & A_{22}^P(\theta) &= \cos^2\theta, \\ A_{11}^S(\theta) &= \cos^2\theta, & A_{12}^S(\theta) &= -\sin\theta\cos\theta, \\ A_{21}^S(\theta) &= \sin\theta\cos\theta, & A_{22}^S(\theta) &= \sin^2\theta. \end{aligned} \tag{19}$$

The primary waves (P waves in this study) generate both scattered P and scattered S waves at the boundaries of heterogeneities due to wavetype coupling, and therefore the total scattered wavefield u_j^s can be represented as a sum of scattered P and S waves (u_j^{PP} , u_j^{PS} where $j = x, z$ or 1, 2). From equations (7), (9), (16), and (17), u_j^{PP} and u_j^{PS} are given by

$$\begin{aligned} u_j^{PP} &= \sqrt{\frac{k_\alpha}{8\pi|\mathbf{x}|}} \exp\left[-i\left(\omega t - k_\alpha|\mathbf{x}| + \frac{\pi}{4}\right)\right] \\ &\cdot \left\{ C_1 A_{j1}^P(\theta) \int_S \frac{\partial \xi}{\partial x} e^{ik_\alpha(z-\mathbf{n}\cdot\mathbf{x}')} dS(\mathbf{x}') \right. \\ &+ 2ik_\alpha A_{j2}^P(\theta) \int_S \xi e^{ik_\alpha(z-\mathbf{n}\cdot\mathbf{x}')} dS(\mathbf{x}') \\ &+ \left. C_2 A_{j2}^P(\theta) \int_S \frac{\partial \xi}{\partial z} e^{ik_\alpha(z-\mathbf{n}\cdot\mathbf{x}')} dS(\mathbf{x}') \right\}, \end{aligned} \tag{20}$$

and

$$\begin{aligned} u_j^{PS} &= \sqrt{\frac{k_\alpha\gamma^3}{8\pi|\mathbf{x}|}} \exp\left[-i\left(\omega t - k_\beta|\mathbf{x}| + \frac{\pi}{4}\right)\right] \\ &\cdot \left\{ C_1 A_{j1}^S(\theta) \int_S \frac{\partial \xi}{\partial x} e^{ik_\alpha(z-\gamma\mathbf{n}\cdot\mathbf{x}')} dS(\mathbf{x}') \right. \\ &+ 2ik_\alpha A_{j2}^S(\theta) \int_S \xi e^{ik_\alpha(z-\gamma\mathbf{n}\cdot\mathbf{x}')} dS(\mathbf{x}') \\ &+ \left. C_2 A_{j2}^S(\theta) \int_S \frac{\partial \xi}{\partial z} e^{ik_\alpha(z-\gamma\mathbf{n}\cdot\mathbf{x}')} dS(\mathbf{x}') \right\}, \end{aligned} \tag{21}$$

where we have written γ for α/β .

The integrals in equations (20) and (21) can be simplified by using integration by parts to yield

$$u_j^{PP} = i \sqrt{\frac{k_\alpha^3}{8\pi|\mathbf{x}|}} \{C_1 A_{j1}^P(\theta) \sin\theta + 2A_{j2}^P(\theta) + C_2 A_{j2}^P(\theta) (\cos\theta - 1)\} \\ \times \exp\left[-i\left(\omega t - k_\alpha|\mathbf{x}| + \frac{\pi}{4}\right)\right] \int_S \xi e^{ik_\alpha(z-\mathbf{n}\cdot\mathbf{x}')} dS(\mathbf{x}'), \quad (22)$$

and

$$u_j^{PS} = i \sqrt{\frac{k_\alpha^3 \gamma^3}{8\pi|\mathbf{x}|}} \{C_1 A_{j1}^S(\theta) \gamma \sin\theta + 2A_{j2}^S(\theta) + C_2 A_{j2}^S(\theta) (\gamma \cos\theta - 1)\} \\ \times \exp\left[-i\left(\omega t - k_\beta|\mathbf{x}| + \frac{\pi}{4}\right)\right] \int_S \xi e^{ik_\alpha(z-\gamma\mathbf{n}\cdot\mathbf{x}')} dS(\mathbf{x}'). \quad (23)$$

In this far-field approximation, the scattered P and S waves can be isolated on a single component (radial or tangential) by rotation of the coordinate axes (e.g., Sato and Fehler, 1998):

$$u_r^{PP} = \sin\theta u_x^{PP} + \cos\theta u_z^{PP} = i \sqrt{\frac{k_\alpha^3}{8\pi|\mathbf{x}|}} C_r(\theta) \\ \exp\left[-i\left(\omega t - k_\alpha|\mathbf{x}| + \frac{\pi}{4}\right)\right] \int_S \xi e^{ik_\alpha(z-\mathbf{n}\cdot\mathbf{x}')} dS(\mathbf{x}'), \quad (24)$$

$$u_t^{PS} = \cos\theta u_x^{PS} - \sin\theta u_z^{PS} = i \sqrt{\frac{k_\alpha^3 \gamma^3}{8\pi|\mathbf{x}|}} C_t(\theta) \\ \exp\left[-i\left(\omega t - k_\beta|\mathbf{x}| + \frac{\pi}{4}\right)\right] \int_S \xi e^{ik_\alpha(z-\gamma\mathbf{n}\cdot\mathbf{x}')} dS(\mathbf{x}'),$$

where $C_r(\theta)$ and $C_t(\theta)$ are

$$C_r(\theta) = \sin\theta \{C_1 A_{11}^P(\theta) \sin\theta + 2A_{12}^P(\theta) + C_2 A_{12}^P(\theta) (\cos\theta - 1)\} \\ + \cos\theta \{C_1 A_{21}^P(\theta) \sin\theta + 2A_{22}^P(\theta) + C_2 A_{22}^P(\theta) (\cos\theta - 1)\}, \\ C_t(\theta) = \cos\theta \{C_1 A_{11}^S(\theta) \gamma \sin\theta + 2A_{12}^S(\theta) + C_2 A_{12}^S(\theta) (\gamma \cos\theta - 1)\} \\ - \sin\theta \{C_1 A_{21}^S(\theta) \gamma \sin\theta + 2A_{22}^S(\theta) + C_2 A_{22}^S(\theta) (\gamma \cos\theta - 1)\}. \quad (25)$$

To extract the average scattered energy, we consider an ensemble average over different realizations of the stochastic medium for the displacement terms:

$$\langle |u_r^{PP}|^2 \rangle = \frac{k_\alpha^3}{8\pi|\mathbf{x}|} [C_r(\theta)]^2 \\ \times \int_S \int_S \langle \xi(\mathbf{x}') \xi(\mathbf{y}') \rangle \exp[ik_\alpha \{\mathbf{e}_z \cdot (\mathbf{x}' - \mathbf{y}') \\ - \mathbf{n} \cdot (\mathbf{x}' - \mathbf{y}')\}] dS(\mathbf{x}') dS(\mathbf{y}'), \quad (26) \\ \langle |u_t^{PS}|^2 \rangle = \frac{k_\alpha^3 \gamma^3}{8\pi|\mathbf{x}|} [C_t(\theta)]^2 \\ \times \int_S \int_S \langle \xi(\mathbf{x}') \xi(\mathbf{y}') \rangle \exp[ik_\alpha \{\mathbf{e}_z \cdot (\mathbf{x}' - \mathbf{y}') \\ - \gamma \mathbf{n} \cdot (\mathbf{x}' - \mathbf{y}')\}] dS(\mathbf{x}') dS(\mathbf{y}'),$$

where \mathbf{e}_z is the unit vector for the z -axis direction. Following the procedure for scalar waves (Frankel and Clayton, 1986; Roth and Korn, 1993), we can rewrite equation (26) using the power spectral density function (k) for the heterogeneity as

$$\langle |u_r^{PP}|^2 \rangle = \frac{k_\alpha^3 S}{8\pi|\mathbf{x}|} [C_r(\theta)]^2 \mathcal{P} \left[2k_\alpha \sin \frac{\theta}{2} \right], \quad (27) \\ \langle |u_t^{PS}|^2 \rangle = \frac{k_\alpha^3 \gamma^3 S}{8\pi|\mathbf{x}|} [C_t(\theta)]^2 \mathcal{P} \left[k_\alpha \sqrt{1 + \gamma^2 - 2\gamma \cos\theta} \right].$$

The derivation of equation (27) from equation (26) is described in detail in Appendix A. The loss factor for scattering attenuation Q_s^{-1} corresponds to the energy loss per unit area divided by the solid angle (2π) and wavenumber, and so we can express Q_s^{-1} in terms of the standard deviation (ε) of velocity fluctuation in the 2D media by

$$Q_s^{-1} = \frac{\varepsilon^2}{2\pi S k_\alpha} \int_\theta \{ \langle |u_r^{PP}|^2 \rangle + \langle |u_t^{PS}|^2 \rangle \} dA, \quad (28)$$

where A is the arc length through which scattered waves propagate, so that dA is given by $r d\theta$ (Frankel and Clayton, 1986).

An approximation for the scattering loss factor Q_s^{-1} can be made by restricting the angular range over which the single scattering theory is applied. For an angular span ($< \theta_{\min}$ about the forward direction) we represent the true multiple scattering effects via a travel-time correction. Since the scattered angles of PP and PS waves from a heterogeneity are different, we introduce θ_{\min}^P for the P -wave-type scattering and θ_{\min}^S for the S -wave-type scattering. Then we can represent Q_s^{-1} with the approximate travel-time correction as

$$Q_s^{-1} = \frac{r\varepsilon^2}{2\pi S k_\alpha} \left\{ \int_{\theta_{\min}^P}^{2\pi - \theta_{\min}^P} \langle |u_r^{PP}|^2 \rangle d\theta \right. \\ \left. + \int_{\theta_{\min}^S}^{2\pi - \theta_{\min}^S} \langle |u_t^{PS}|^2 \rangle d\theta \right\}. \quad (29)$$

When $|\mathbf{x}|$ is large enough, we can assume $|\mathbf{x}| \approx r$. Also, θ_{\min}^S can be represented in terms of θ_{\min}^P by using the Snell's law; for PP scattered waves reflected with the minimum scattering angle θ_{\min}^P from the boundary of heterogeneity, the corresponding reflection angle of PS scattered waves can be calculated for single scattering as (see Fig. 2)

$$\theta_{\min}^S = \theta_{\min}^P + (\phi_P - \phi_S), \quad \text{where } \phi_P \\ = \frac{\pi - \theta_{\min}^P}{2}, \quad \phi_S = \sin^{-1} \left(\frac{\sin\phi_P}{\gamma} \right). \quad (30)$$

Therefore, when we set k_α to be k , θ_{\min}^P to be θ_{\min} , and $\Delta\phi$ to be $(\phi_P - \phi_S)$, the approximate relationship between Q_s^{-1} and ka for elastic waves is given with implicit dependence on a through \mathcal{P} by

$$\begin{aligned}
 \frac{Q_s^{-1}}{\varepsilon^2} &= \frac{k^2}{(4\pi)^2} \int_{\theta_{\min}}^{2\pi-\theta_{\min}} [C_t(\theta)]^2 \mathcal{P} \left[2k \sin \frac{\theta}{2} \right] d\theta \\
 &+ \frac{k^2 \gamma^2}{(4\pi)^2} \int_{\theta_{\min}+\Delta\phi}^{2\pi-\theta_{\min}-\Delta\phi} [C_t(\theta)]^2 \mathcal{P} \left[k \sqrt{1 + \gamma^2 - 2\gamma \cos\theta} \right] d\theta.
 \end{aligned} \quad (31)$$

Comparison with Results from Scalar Wave Approximation

We have derived the scattering attenuation formula for 2D elastic waves in terms of normalized wavenumber (ka) for stochastic media where the physical parameters (Lamé coefficients and density) are varied randomly. There are significant differences in the characteristics of elastic waves and scalar waves, particularly in radiation patterns associated with scattering, the phase coupling on a boundary of heterogeneity, and the differences in the frequency content of P and S waves. We therefore expect noticeable differences in the scattering induced for scalar and elastic waves.

We compare the scattering attenuation formula for elastic waves with that for scalar waves (Frankel and Clayton, 1986) and discuss possible problems when the theoretical attenuation curve for scalar waves is used instead of that for elastic waves. For convenience, we consider a case only with velocity perturbations, such as $K = 0$ in equation (6). The theoretical scattering attenuation formula as a function of ka for scalar waves is then given by (Frankel and Clayton, 1986; Frenje and Juhlin, 2000)

$$Q_s^{-1} = \frac{k^2 \varepsilon^2}{\pi} \int_{\theta_{\min}}^{\pi} \mathcal{P} \left[2k \sin \frac{\theta}{2} \right] d\theta, \quad (32)$$

where ε is the standard deviation of the velocity perturbation.

The theoretical expression for the scattering attenuation for elastic waves in equation (31) includes both the wavenumber for P waves and the ratio (γ) of P - and S -wave velocities, which means that the Poisson's ratio is an important factor in the scattering process of elastic waves. This is illustrated in Figure 3, where we compare the theoretical scattering attenuation curves for elastic waves with different P/S velocity ratios (γ) for a random medium with a von Karman distribution with a Hurst number (ν) of 0.25. We consider a constant background P -wave velocity of 6.74 km/sec. In the figure, the elastic scattering curves are plotted together with the curve for scalar waves for which θ_{\min} is 30° . There is a significant dependence of the scattering attenuation behavior as a function of the velocity ratio γ as γ is increased, the normalized wavenumber for the peak attenuation is reduced and also the magnitude of the attenuation tends to increase. Although the attenuation curve for scalar waves displays a similar pattern to that for elastic waves with $\gamma = 1.75$, which is a plausible velocity ratio in the crust, the attenuation levels for elastic waves are smaller than those for scalar waves for large ka . It is therefore preferable to

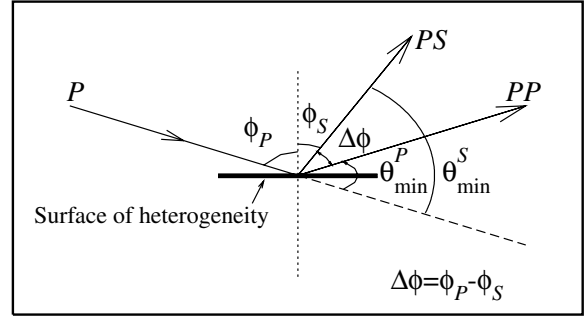


Figure 2. The determination of the minimum scattering angle for S waves θ_{\min}^S in terms of θ_{\min}^P using Snell's law. P wave is incident with angle ϕ_P to the normal to the surface of heterogeneity and the PP scattered wave is reflected at the surface with angle θ_{\min}^P to the incident direction (z -axis direction in this study). The PS scattered wave is reflected on the surface with angle ϕ_S to the normal and τ_{\min}^S to the incident direction.

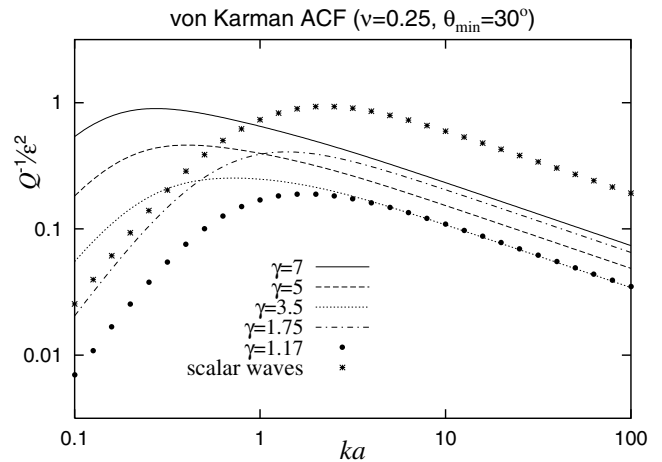


Figure 3. Comparison of theoretical scattering attenuation (Q^{-1}) curves with the minimum scattering angle (θ_{\min}) of 30° for scalar waves and elastic waves with various ratios ($\gamma = 1.17, 1.75, 3.5, 5, 7$) of P - and S -wave velocities in von Karman random media with the Hurst number (ν) of 0.25. The reference P -wave velocity is set at 6.74 km/sec. The theoretical curves for elastic waves are highly dependent on the velocity ratio.

derive scattering attenuation relations directly for elastic waves rather than rely on the scalar wave results.

Wavelet-Based Method

Hong and Kennett (2002a,b) have introduced a wavelet-based method (WBM) for numerical modeling of elastic waves and have discussed its features in some detail. We therefore summarize the basic scheme of the method and demonstrate its merits for modeling random media with significant velocity variation.

One of the advantages of working with wavelets is the confinement in space and time domains; this allows the representation of differentiation of a function to arbitrary accuracy using a set of wavelet bases (i.e., differential operators are treated using wavelets; Beylkin, 1992). To exploit these wavelet forms for numerical differentiation, we recast the governing elastic wave equations as a set of linked first-order partial differential equations in time by implementing a velocity-displacement formulation. The vector equation system can then be solved with a recursive discrete time solution with the help of a semigroup approach and a Taylor expansion for the exponential function with a matrix operator. Although an approximation of the Taylor expansion is needed to obtain the discrete time solution, the approximation order controls the size of the time step, not the accuracy of numerical responses of elastic waves. One of the outstanding characteristics of WBM, compared with Fourier methods, which can also achieve high accuracy differentiation, is that WBM can implement the free-surface condition exactly and easily by the use of equivalent force terms. These equivalent force terms do not distort the energy conservation of the system so the system is stable in time.

We now consider some aspects of numerical modeling to display the efficiency of the WBM as a simulator of elastic wave propagation in random media. In every numerical method, to achieve accurate and stable results without numerical dispersion requires the size of the grid steps to depend on the frequency content of source time function and the wave velocities in the medium. In particular, the number of grid points needed for the smallest expected wavelength expected in the media will determine the size of the required grid and the consequent computational effort. Hence the number of grid points per wavelength is often used to present the efficiency of given method as a numerical simulator (Komatitsch and Vilotte, 1998). The fourth-order FDM requires at least 10 grid points per wavelength in models with strong impedance contrast between layers (Shapiro *et al.*, 2000), while WBM using Daubechies-20 wavelets needs 3 grid points per wavelength (see Hong and Kennett, 2002a). These grid steps are sufficient to produce stable and accurate results in simple media. However, it is necessary to check whether these methods can generate accurate responses in complex media such as random media. In complex media, we expect sharp changes in physical parameters between grid points and so resolution of physical changes is an important issue, as is the accuracy of differentiation.

We first consider the process of differentiation in a random medium and then present examples of WBM modeling in the presence of very strong heterogeneity. In a random medium we can expect strong variations in properties, and we can simulate the effects by taking discrete samples of a rapidly varying function $f(x)$ on 1D domain x for example, $f(x)$ can be considered as a displacement field combined with highly perturbed Lamé coefficients (e.g., λu_x) in the media. We use the functional form (Fig. 4a):

$$f(x) = x^3 \sin(x\sqrt{x}) \exp\left(-\frac{x}{2}\right), \quad (33)$$

and the analytic derivative $f'(x)$ is (Fig. 4b)

$$f'(x) = \frac{3}{2} x^{7/2} \cos(x\sqrt{x}) \exp\left(-\frac{x}{2}\right) + (3x^2 - \frac{1}{2} x^3) \sin(x\sqrt{x}) \exp\left(-\frac{x}{2}\right), \quad (34)$$

where $0 < x \leq 20$ and x corresponds to the dimensionless distance in the domain. For the numerical differentiation, we implement both the fourth-order FDM and the WBM. When the signal $f(x)$ is considered on a sufficiently dense grid system (e.g., number of grid points $N_x = 256$, grid step $\delta x = 0.0781$), both numerical estimates of the derivative ($f'(x)$) are apparently coincident with the analytical solution. However, for a sparser grid system with $N_x = 64$ ($\delta x = 0.3125$), the derivative estimates from the FDM exhibit attenuated amplitudes while WBM generates correct responses. This example of the differentiation of $f(x)$ on the sparse grid system would correspond physically to the situation of a medium with high fractional fluctuation or where diverse strong heterogeneities are present in a given area. Thus, FDM may generate attenuated results for fine-scale heterogeneities or when a high fractional fluctuation is considered in the random media.

This phenomenon has previously been reported in a study based on FDM for modeling in random media; Jannaud *et al.* (1991) have shown that the measured scattering attenuation rates exhibit high attenuation relative to the theoretically expected rates when a high fractional fluctuation is considered in the random media ($\varepsilon = 10\%$, 20% in their study). However, there was good agreement between numerical and theoretical results for the case of a weakly perturbed medium ($\varepsilon = 4\%$). In the presence of high levels of fluctuations, the smoothness assumptions underlying the FDM forms of the numerical operators for differentiation break down, with the result that artificially attenuated wavefields are produced. The WBM, on the other hand, considers the differentiation of the whole data at all grid points through wavelet decomposition on a set of spaces (i.e., the variations of high-frequency content and low-frequency content are handled in separate spaces but at the same time) and therefore retains accuracy throughout the domain without accumulating numerical errors across the grid.

As a further demonstration of the efficacy of the WBM, we consider the stability of the calculations for highly perturbed media. For this test, two kinds of models with high-velocity perturbations are considered: (1) a pointwise random medium (Fig. 5a) where wave speeds vary randomly with the Gaussian probability distribution with a standard deviation of velocity perturbation of 20% and (2) a systematic random medium generated by von Karman autocorrelation function (ACF) with a Hurst number (ν) of 0.25 (Fig.

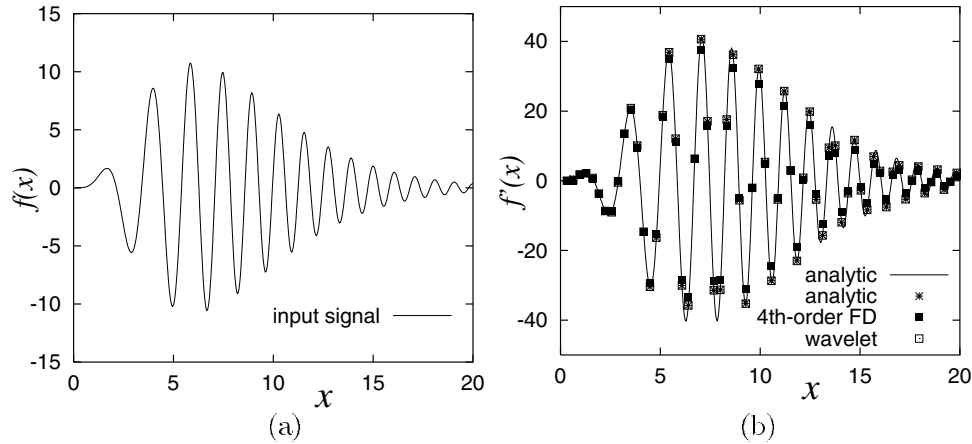


Figure 4. Comparison of the accuracy of differentiation between the fourth-order finite difference method (FDM) and the wavelet-based method (WBM): (a) highly varying input signal that corresponds to the variation of physical parameters in random media and (b) numerical results which show that the fourth-order FDM exhibits the attenuated results for the derivative, but WBM generates very accurate results even when the number of discretization points for the input signal is decreased to 64.

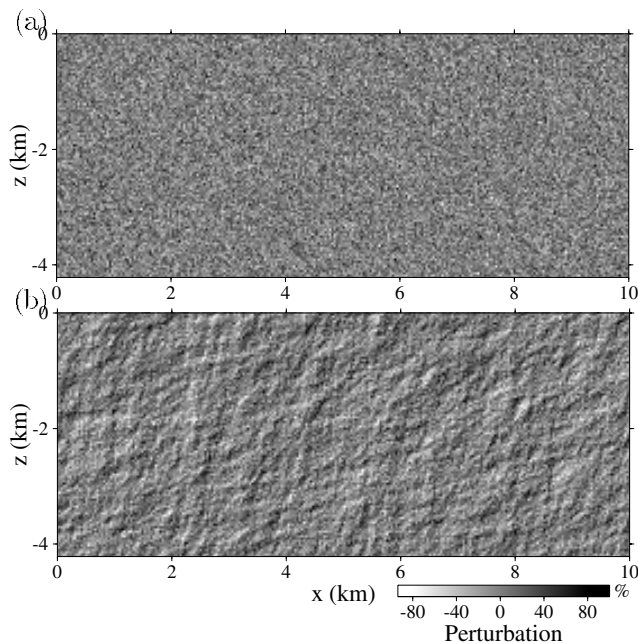


Figure 5. Representation of (a) a pointwise random heterogeneous medium with a standard deviation of velocity perturbation of 20% and (b) a stochastic random heterogeneous medium generated by von Karman ACF with the Hurst number (ν) of 0.25, a correlation distance of 100 m and a standard deviation of velocity perturbation of 52%.

5b), a correlation distance of 100 m, and a standard deviation of velocity perturbation of 52%. The maximum value of the velocity perturbations reach 98% for the pointwise medium and 92% for the von Karman medium. For such high levels of perturbation, the conventional FDM is subject to strong

dispersion in the numerical results (M. Roth, personal comm., 2001).

The reference P - and S -wave speeds for the WBM calculation are 3.5 and 2.0 km/sec, and a vertically directed point force is applied at depth 1500 m in a 10×5 km² domain. Forty-two receivers deployed at the free surface collect the time responses. Despite the large variations in the physical parameters, the WBM generates stable time responses with large coda waves following the main phases for both the pointwise and stochastic random heterogeneous media (Fig. 6). Since the scattering effects depend on both the frequency content of source time function and the scale of heterogeneities, the coda waves in pointwise random media are smaller than those in the stochastic random media.

These two experiments demonstrate that the WBM can generate accurate and stable results in even strongly heterogeneous random media. We are therefore able to undertake the simulation of elastic wave propagation in different styles of random heterogeneous media and measure the scattering attenuation factors by assessing the scattered energy.

Construction of Stochastic Random Media

A number of studies have been made of the theoretical conditions on media so that the scattering of elastic waves can be represented effectively with the first-order Born approximation, that is, single scattering (Kennett, 1972; Aki and Richards, 1980; Hudson and Heritage, 1981; Wu and Aki, 1985). When comparisons are to be made with the results of numerical models, it is particularly important that an exact representation is made of a specific random medium. Recently, Frenje and Juhlin (2000) have presented theoretical conditions for implementation of a valid correlation distance in a discretized spatial medium. They have derived the

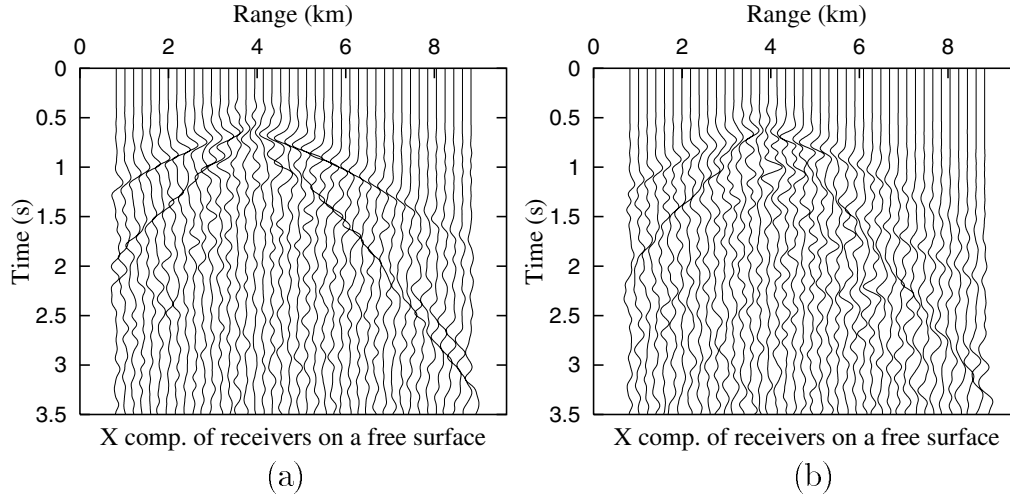


Figure 6. Time responses of the horizontal components of displacement at the free surface receivers for the highly perturbed models shown in Figure 5: (a) the pointwise random medium and (b) the stochastic random medium.

conditions between the grid steps (δx , δz) and the correlation distance (a) on the basis that the minimum wavenumber ($k_{\min}^j = 2\pi/l_j$, $j = x, z$, $l_j =$ length of domain in j direction) is smaller than the corner wavenumber ($k_c = 1/a$), and the Nyquist wavenumber ($k_{\text{nyq}}^j = \pi/\delta j$, $j = x, z$) is larger than the corner wavenumber. However, models based on the autocorrelation function (ACF) do not depend on the corner wavenumber (Mai and Beroza, 2002), and so it is necessary to check the suitability of a specific random medium by considering both the limits on the accuracy of the numerical differentiation and the representation of the medium with a given correlation distance. The accuracy requirement determines the smallest acceptable size of the heterogeneities in domain, and the physical limits of the model control the maximum acceptable size.

The WBM will remain stable in a pointwise medium with large fluctuations for correlation distances down to $a = \max\{\delta x, \delta z\}/8$. The FDM needs a correlation distance that is sufficiently large compared with the grid steps (i.e., $\max\{\delta x, \delta z\} \ll a$; see Frenje and Juhlin, 2000). The physical limit comes from the confinement in size when using a limited number of grid points to represent the medium. When random heterogeneities with large correlation distance are placed in a relatively small medium, the heterogeneities behave as a “virtual structure” and generate biased results (e.g., Frankel and Clayton, 1986). Therefore, it is necessary to check whether the fractional fluctuation of physical parameters generated by a model is appropriate for the numerical representation of given random medium.

For this purpose, we introduce a measure of “randomicity rate” (C_N), which will be close to zero when the domain is sufficiently large compared with the heterogeneities. We define

$$C_N = \frac{|N_+ - N_-|}{N_+ + N_-} \sim 0, \quad (35)$$

where N_+ and N_- are the numbers of grid points with positive and negative random values for the fractional fluctuation of physical parameters. When the domain is large enough, the positive and negative random values are distributed homogeneously (i.e., $N_+ \approx N_-$ in the domain) and C_N becomes close to 0.

In addition to these conditions, the distance from source to receiver is another important factor for the accurate measurement of scattering attenuation; since waves propagating through a random medium experience focusing and defocusing effects, the travel times and amplitudes of waves recorded at short distances from the source are very variable (Hoshiya, 2000). The time responses for short distances are thus not very suitable for a quantitative study. We therefore endeavored to set the receivers at a sufficient distance that the influence of the heterogeneity tends to minimize the variations in amplitudes between different receivers. For this purpose we introduced a domain that is composed of 512-by-512 grid points corresponding to $77 \times 77 \text{ km}^2$ ($\delta x = \delta z = 150.3 \text{ m}$) in physical space (Fig. 7). The plane P -wave source is located at the 70th grid point from the bottom boundary Γ_B (i.e., $z = 10.5 \text{ km}$), and the receivers are set at the 70th grid point from the top boundary Γ_T . The 128 receivers are deployed horizontally with uniform spacing at every fourth grid point (i.e., $x = 0.6 \text{ km}$). The reference compressional wave velocity (α_0) is 6.74 km/sec, the shear wave velocity (β_0) is 3.85 km/sec, and the density (ρ_0) is 2.9 g/cm³, which are typical crustal values (cf., Kennett *et al.*, 1995). The source time function is a Ricker wavelet with dominant frequency (f_c) 4.5 Hz. The top and bottom artificial

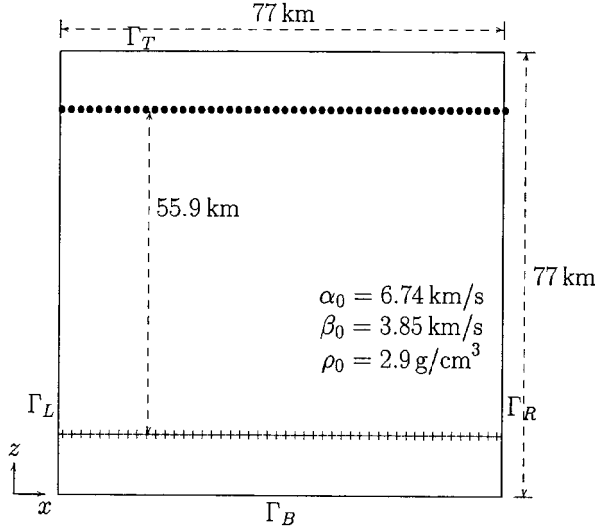


Figure 7. Configuration of a 2D unbounded medium with 128 receivers (●) placed with uniform interval (602 m) at 10.5 km from the top boundary (Γ_T). A plane P -wave source (+) is located at 10.5 km from the bottom boundary (Γ_B). The reference compressional (α_0) and shear (β_0) wave velocities are 6.74 and 3.85 km/sec, and the reference density (ρ_0) is 2.9 g/cm³. The top and bottom artificial boundaries (Γ_T , Γ_B) are treated by absorbing boundary conditions and the left and right boundaries (Γ_L , Γ_R) are considered with periodic boundary conditions.

boundaries (Γ_T , Γ_B in Fig. 7) are treated with absorbing boundary conditions, and the other boundaries (Γ_R , Γ_L) by periodic boundary conditions to imitate a domain with the unlimited horizontal length. For more detail of implementation of absorbing boundary conditions and periodic boundary conditions, refer to Hong and Kennett (2002a,b).

We constructed stochastic random media using von Karman, exponential, and Gaussian autocorrelation functions (ACF, $N(r)$) and their power spectral density functions (PSDF, $\mathcal{P}(k)$). The von Karman ACF and PSDF in 2D media are (e.g., Sato and Fehler, 1998)

$$N(r) = \frac{1}{2^{\nu-1}\Gamma(\nu)} \left(\frac{r}{a}\right)^{\nu} K_{\nu}\left(\frac{r}{a}\right), \quad (36)$$

$$\mathcal{P}(k) = \frac{4\pi\nu a^2}{(1 + k^2 a^2)^{\nu+1}},$$

where r is a spatial lag, a is the correlation distance, ν is the Hurst number, Γ is the Gamma function, k is a wavenumber, and K_{ν} is the modified Bessel function of order ν . The exponential ACF and PSDF are

$$N(r) = e^{-r/a}, \quad \mathcal{P}(k) = \frac{2\pi a^2}{(1 + k^2 a^2)^{3/2}}, \quad (37)$$

and the Gaussian ACF and PSDF are given by

$$N(r) = e^{-r^2/a^2}, \quad \mathcal{P}(k) = \pi a^2 e^{-k^2 a^2/4}. \quad (38)$$

Note that the exponential ACF corresponds to the von Karman ACF with Hurst number 0.5.

To generate the stochastic random models, we use the PSDF, the spectrum of the ACF, in the wavenumber domain (Roth and Korn, 1993) and assign random numbers distributed evenly between $-\pi$ and π to the phase $\Phi(k_x, k_z)$ at each point (k_x, k_z) . The fractional fluctuation of velocities in the wavenumber domain $\bar{\xi}(k_x, k_z)$ is then expressed as

$$\bar{\xi}(k_x, k_z) = \sqrt{l_x l_z} \sqrt{P(k_r)} e^{i\Phi(k_x, k_z)}, \quad (39)$$

where k_r is the root mean square of k_x and k_z , and l_j ($j = x, z$) is the extent of the medium in the j direction. The resultant fractional fluctuation of the velocities in spatial domain $\xi(x, z)$ in equation (6) is obtained by 2D Fourier transforms. We consider 10% standard deviation ε for the wave-speed perturbation, and following Sato (1984) set $K = 0.8$ in equation (6) to control the perturbation level for the density.

Scattering Patterns and Process

We undertook numerical modeling of elastic waves in stochastic heterogeneous media with three different styles: (a) generated by von Karman ACFs with $\nu = 0.05$ and 0.25 , (b) exponential ACF (corresponding to von Karman ACF with $\nu = 0.5$), and (c) a Gaussian ACF. Each type of random media is considered for six different values of the correlation distances ($a = 34, 85.4, 214.5, 538.7, 1353.2, 3399$ m). In this situation, the normalized wavenumbers ($k_d a$) for the dominant frequency (4.5 Hz in this study) of incident waves are 0.14, 0.36, 0.90, 2.26, 5.68, and 14.26. The scattering attenuation for each case is measured from a band of normalized wavenumbers including $k_d a$. The smallest correlation distance implemented in this study, $a = 34$ m, satisfies the required condition, $a \geq \max\{\delta x, \delta z\}/8$, for the application of the WBM. In Table 1, we present the randomness rate (C_N) for each of the simulations. The C_N values increase with the size of correlation distances in von Karman and exponential media, but for the simulation of Gaussian media show a complicated pattern (see, C_N values for Gaussian media at $a = 538.7$ m).

To obtain a good assessment of the scattering attenuation we needed to take into account the nature of the scattered signal. For vertically incident plane P waves on media with small-scale heterogeneities, the primary waves are mostly recorded at the z component and the x component contains mostly scattered waves (see Fig. 8). In this case, the scattering attenuation can be measured by considering the energy loss of the incident waves on z -component records. However, in a medium with large-scale heterogeneity, there can be significant deviations in the directions of the primary waves. Thus, for example, in the synthetic seismograms for the Gaussian random medium with $a = 1353.2$,

Table 1
 Numbers of Grid Points with Positive and Negative Values (N_+ , N_-) for the Random Variation for the Reference Physical Parameters of the Stochastic Random Media and the Randomicity Rate C_N as a Function of the Correlation Distance (a)

$a(m)$	34	85.4	214.5	538.7	1353.2	3399
● von Karman ($\nu = 0.05$)						
N_+	131550	131545	131659	132080	132893	135024
N_-	130594	130599	130485	130064	129251	127120
C_N	0.0036	0.0036	0.0045	0.0077	0.0139	0.0302
● von Karman ($\nu = 0.25$)						
N_+	131522	131551	131796	132395	133365	136339
N_-	130622	130593	130348	129749	128779	125805
C_N	0.0034	0.0037	0.0055	0.0101	0.0175	0.0402
● von Karman ($\nu = 0.5$, exponential)						
N_+	131422	131542	132002	132548	133591	137422
N_-	130722	130602	130142	129596	128553	124722
C_N	0.0027	0.0036	0.0071	0.0113	0.0192	0.0484
● Gaussian						
N_+	131383	131389	131637	132164	131641	132593
N_-	130761	130755	130507	129980	130503	129551
C_N	0.0024	0.0024	0.0043	0.0083	0.0043	0.0116

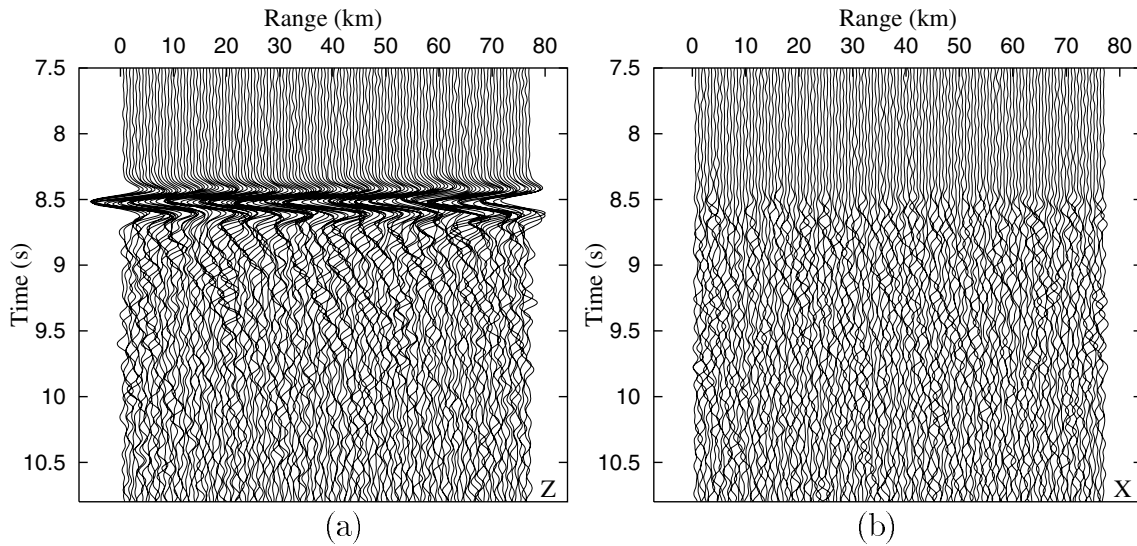


Figure 8. Synthetic seismograms from the modeling in the von Karman random media with $\nu = 0.25$ and $a = 214.5$ m. Random scattered waves are developed following the primary waves in z -component seismograms, and mainly scattered waves are recorded on the x component.

3399 m (Fig. 9), the primary waves recorded on the z component display a systematic change of amplitudes and arrival times, which is also mirrored on the x -component seismograms. A similar phenomenon is found in seismograms from von Karman (also exponential) random media with large scale of heterogeneities (see Fig. 10), where systematically deviated waves develop clearly ahead of the scattered coda. However, the systematic variation becomes noticeably reduced for a von Karman medium with small value of Hurst number (see Fig. 11). The level of scattered waves generated is related to the spectral filtering introduced by the particular

autocorrelation function (Klimeš, 2002). For example, there are less scattered waves for a Gaussian media with a large correlation distance because the band of wavenumber coupling scales as $1/a$.

The scattering attenuation rate is measured in from the seismograms calculated for the random media using a spectral ratio approach (Aki and Richards, 1980):

$$Q_s^{-1}(\omega) = \frac{2c}{\omega r} \ln \left[\frac{A_0(\omega)}{A_r(\omega)} \right], \quad (40)$$

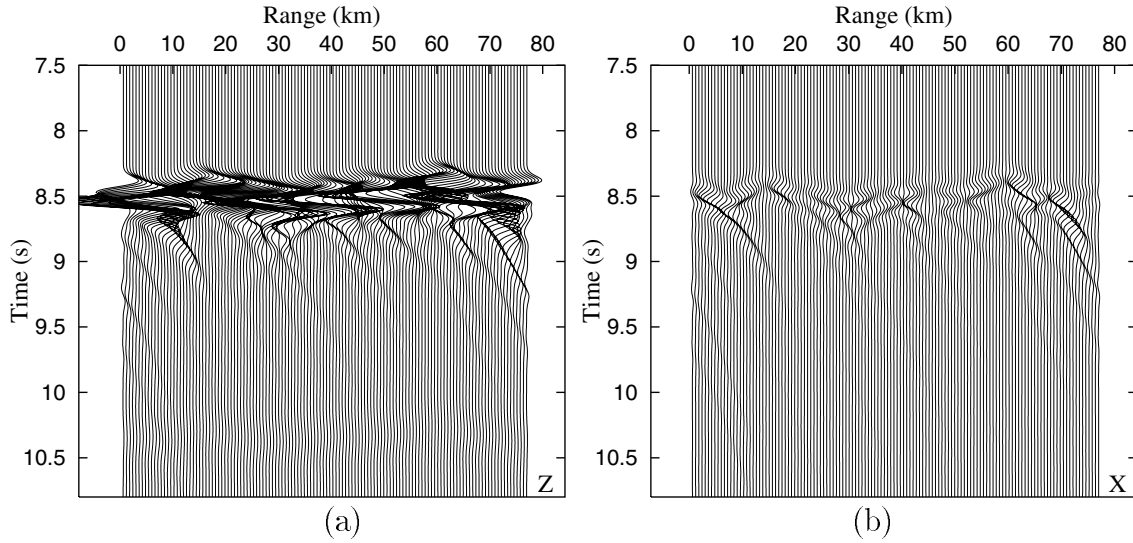


Figure 9. Synthetic seismograms from the modeling in Gaussian random media with $a = 3399$ m. The seismograms are composed of mainly primary waves without random scattered waves. The primary waves are recorded on both x and z components since the waves deviate from the incident direction due to influence of the large scale of the heterogeneity.

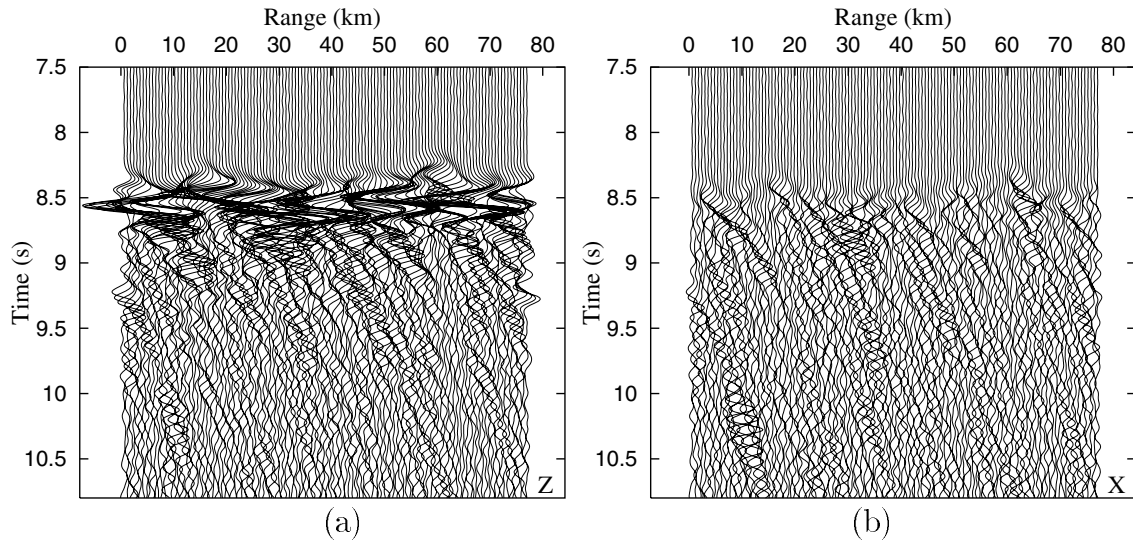


Figure 10. Synthetic seismograms from the modeling in exponential random media with $a = 1353.2$ m. The primary waves are recorded on both x and z components with background random scattered waves.

where c is the wave speed, r is the spatial lag, and $A_0(\omega)$ and $A_r(\omega)$ are spectral amplitudes of waves for angular frequency ω at the origin and at the receiver. The spectral amplitudes of the primary waves are estimated by stacking 128 seismograms in the frequency domain. These seismograms are tapered in the time domain using a “cosine bell” (Kanasewich, 1981), (Fig. 12) to isolate primary waves from scattered waves. The time length L_1 and L_2 are measured from the maximum amplitude position (P_{max}), and M controls the tapering rate at the edges of the window.

The parameters of the tapering need to be adapted to the nature of the seismograms, and so we used a constant size of cosine bell with $L_1 = 0.22$ sec, $L_2 = 0.18$ sec, for the calculations with $k_d a = 0.14, 0.36, 0.90,$ and 2.26 ; for the other cases (i.e., $k_d a = 5.68, 14.26$) we used $L_1 = 0.22 \sim 0.5$ sec, $L_2 = 0.18 \sim 0.5$ sec. M kept constant at 0.07 sec. For cases with large-scale heterogeneity, it is necessary to consider both the x - and z -component data. As indicated in Figure 13, the amount of energy on the x component is too large to be ignored in estimates of scattering attenuation,

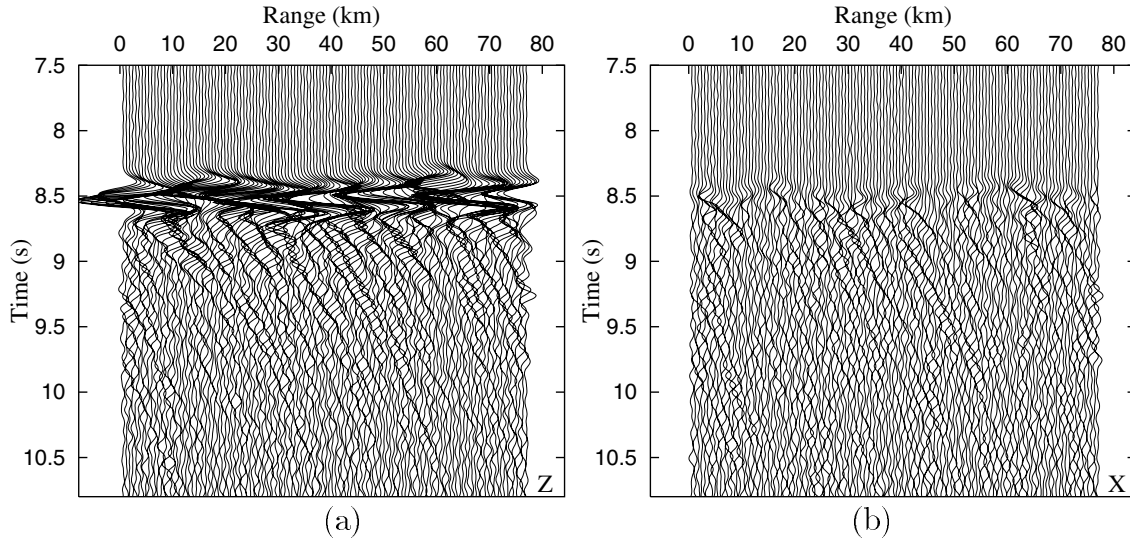


Figure 11. Synthetic seismograms from the modeling in the von Karman random media with $\nu = 0.05$ and $a = 3399$ m. The primary waves is not discernible and mainly random scattered waves are recorded on the x component even the heterogeneity (cf., Fig. 10).

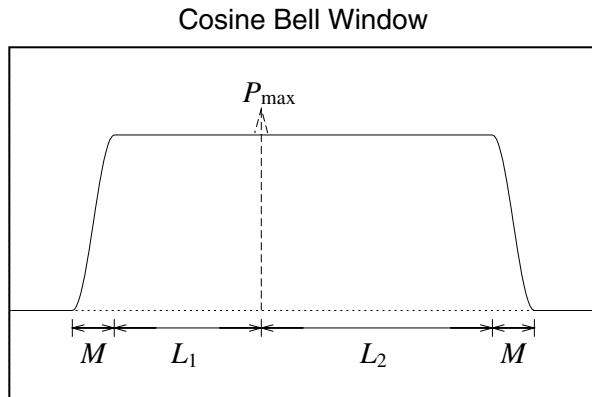


Figure 12. The cosine bell window for tapering seismograms in time domain. P_{max} is the point where the amplitude of seismogram is largest, L_1 and L_2 determine the window size, and M controls the tapering rate at the ends of windows.

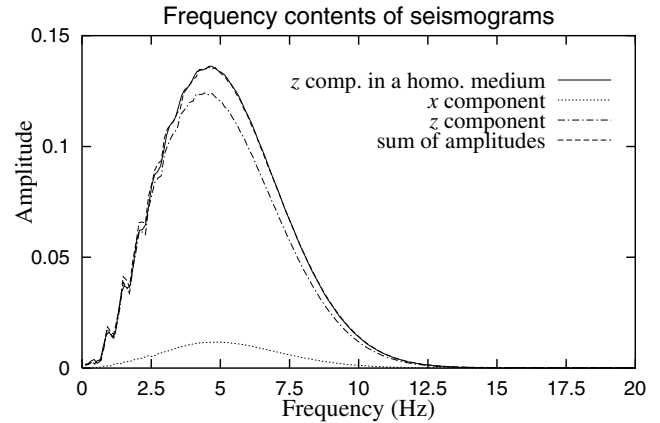


Figure 13. Frequency content of seismograms obtained from modeling in the Gaussian random media with $a = 3399$ m. Significant energy of primary waves is recorded in x component, and the sum of spectral amplitudes in x - and z -component data recover the spectral amplitudes expected in a homogeneous medium.

since otherwise we would get an exaggerated loss by considering only the z component.

Therefore, in some case, such as Gaussian and exponential media with $k_d a = 5.68, 14.26$, and von Karman media with $\nu = 0.25$ and $k_d a = 14.26$, the scattering attenuation is measured by using dual component data and compared with single-component processing. The dual-component processing uses the sum of spectral amplitudes of x - and z -component seismograms (cf. Fig. 13). However, since the data on the x component are composed of both scattered and primary waves, appropriate tapering is required. For each case, the scattering attenuation is measured for a range of frequency from 2 to 9.5 Hz, and the results are displayed around the corresponding $k_d a$ in the $Q_s^{-1} - ka$ diagram.

Comparisons between Theory and Numerical Results

The scattering attenuation for the stochastic random media is measured from the synthetic seismograms for each case and compared with theoretical results in Figure 14. Satisfactory results from a single realization of a stochastic medium can be obtained when $C_N \leq 0.05$. The cases with the different normalized wavenumbers are indicated by different symbols: an open triangle for $k_d a = 0.14$, a filled square for $k_d a = 0.36$, an open circle for $k_d a = 0.90$, a star for $k_d a = 2.26$, an open square for $k_d a = 5.68$, and a filled circle for

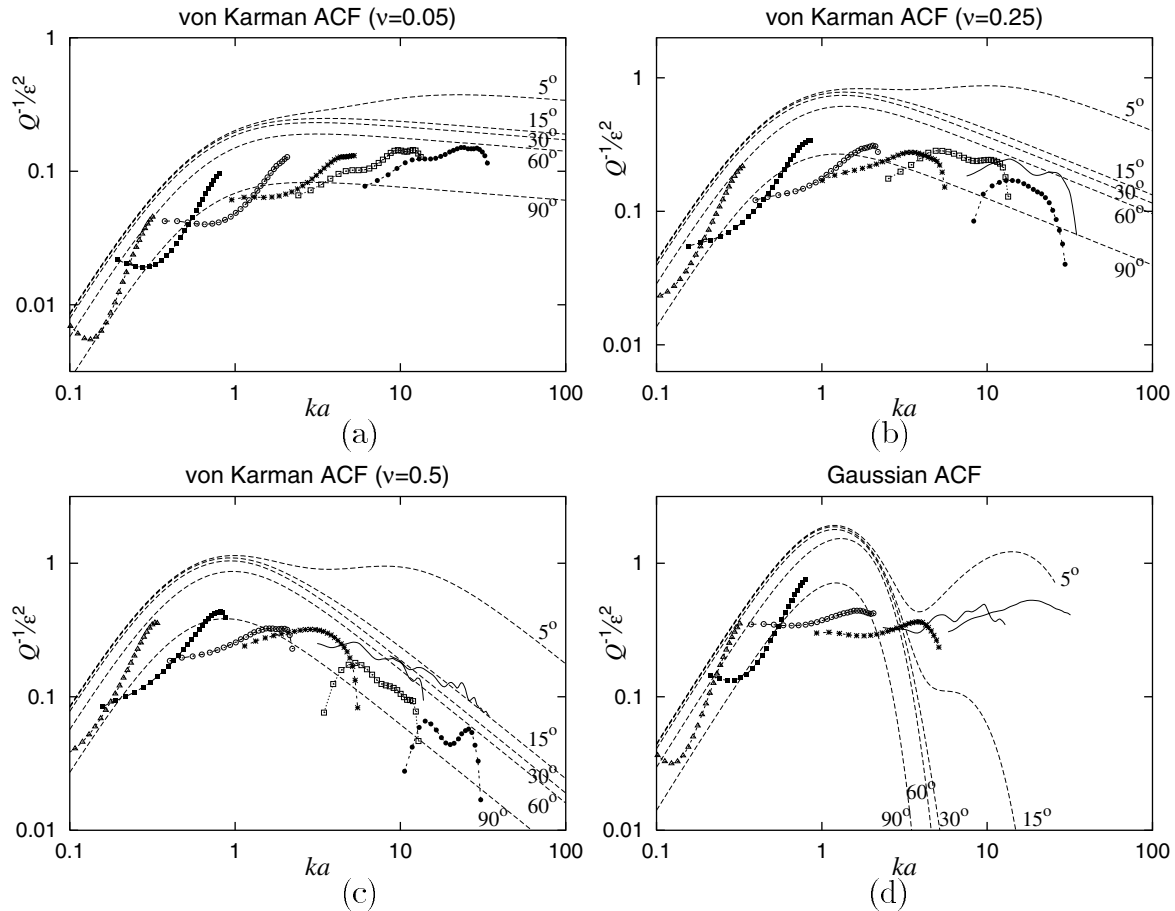


Figure 14. Scattering attenuation factor Q^{-1} normalized for the variance ε^2 as a function of normalized wavenumber ka in the von Karman random media with the Hurst number (a) $\nu = 0.05$, (b) 0.25 , (c) 0.5 (corresponding to the exponential random media) and (d) in the Gaussian random media. The symbols represent the data sets used for calculation of the scattering attenuation. The scattering attenuation measured by using single-component data is provided by solid lines for comparison with that measured by using dual component data. The minimum scattering angle is determined as lying in the range 60° – 90° .

a medium with $k_d a = 14.26$. The scattering attenuation rates measured just from z component data are shown by solid lines, when the symbols represent the use of dual-component data. The discrepancy between the single- and dual-component estimates of attenuation increases with the scale of the heterogeneity and is also dependent on the style of random media. The Gaussian media displays significant discrepancy and the discrepancy also increases with the value of the Hurst number implemented in von Karman media (including exponential media). This reflects the increasing deviation of the P wave from the incident direction with increasing a and ν . Measurements of single-component data may therefore give an overestimate of the scattering attenuation (especially for a Gaussian random media with large-scale heterogeneity).

The measured scattering attenuation rates from each set of data agree well with the trend of the theoretical curves from single scattering theory. The scattering attenuation val-

ues lie within the band for minimum scattering angles (θ_{\min}) between 60° and 90° for all the random media tested. The results from modelling for random media with short correlation distances (e.g., $k_d a = 0.14, 0.36, 0.90$) show a parabolic variation as a function of the normalized wavenumber.

Clearly the minimum scattering angle (θ_{\min}) depends on the particular nature of the stochastic medium but is not less than 60° . This fully elastic result needs to be compared with previous studies that have often used scalar approximations. Sato (1982) predicted θ_{\min} to be 29° for scalar waves based on a cutoff wavelength for decomposition of the fractional fluctuation into long and short wavelengths at twice of the dominant wavelength. Recently, Kawahara (2002) gave a theoretical estimate of θ_{\min} as 65° in 2D acoustic media by considering the phase velocity of travel time corrected mean waves in high-frequency limit. With a help of numerical modeling based on FDM, Frankel and Clayton (1986) measured θ_{\min} as 30° – 45° in 2D elastic media (von Karman,

exponential, Gaussian media), Jannaud *et al.* (1991) estimated 90° in 2D acoustic Gaussian media with weak perturbation (4%) on velocity, Roth and Korn (1993) suggested 20° – 40° in 2D anisotropic acoustic media, and recently Frenje and Juhlin (2000) computed the θ_{\min} for 2D and 3D acoustic media (von Karman, exponential, Gaussian media) as 10° – 20° .

The results of this study are similar to theoretical results of Kawahara (2002) and also close to the numerical study based on FDM in weakly perturbed acoustic media (Jannaud *et al.*, 1991).

Discussion and Conclusions

We established a consistent approach to estimating scattering attenuation for elastic waves using multicomponent information and fully elastic analytic results. We formulated the scattering attenuation variation (Q_s^{-1}) for 2D elastic waves in terms of normalized wavenumber (ka) for stochastic random media. The theoretical scattering attenuation rates of elastic waves are highly dependent on the ratio of P - and S -wave velocities; so it is necessary to use a full elastic treatment rather than use scalar results as a reference.

Accurate numerical modeling is critical for quantitative assessment of stochastic media. Through an example of numerical differentiation, we have shown that there is a possibility of excessive attenuation in rapidly varying media when the smoothness assumptions built into FDM methods are violated. We have shown that the wavelet-based method (WBM) can achieve high accuracy in numerical differentiation and stability in highly perturbed media and so is very suitable for work on scattering attenuation.

Synthetic seismograms have been computed for four types of random media (Gaussian, exponential, and von Karman media with $\nu = 0.05, 0.25$) with six different correlation distances. Large-scale heterogeneity energy in the primary waves gets transferred to the perpendicular to the incident direction; this means that dual-component seismograms are needed for correct measurement of scattering attenuation. For the broad range of stochastic models, the minimum scattering angle for elastic waves, derived from comparison of the WBM with theoretical curves, lies in a band from 60° to 90° . This range of values is similar to those presented by Kawahara (2002) and Jannaud *et al.* (1991) for 2D acoustic media.

The discrepancies in previous results, $\theta_{\min} = 90^\circ$ in mildly perturbed media (4%) and 20° – 30° in more highly perturbed media, may well arise from limitations in previous numerical modeling. The limitations of the FDM can give rise to overestimates of attenuation in media with strong variations.

Acknowledgments

We are grateful to Dr. Michael Fehler (the editor), Dr. Haruo Sato, and an anonymous reviewer for the fruitful comments that improved the

presentation of this article and also to Dr. Michael Roth for comments regarding the use of the FDM in the simulation of scattering. We thank the Australian National University Supercomputer Facility for the use of Alpha server for most of the computations in this study.

References

- Aki, K., and P. G. Richards (1980). *Quantitative Seismology, Theory and Methods*, Vol. 1, W.H. Freeman and Company, San Francisco.
- Arfken, G. (1985). *Mathematical Methods for Physicists*, Third Ed., Academic Press, New York.
- Beylkin, G. (1992). On the representation of operators in bases of compactly supported wavelets, *SIAM J. Numer. Anal.* **6**, 1716–1740.
- Birch, F. (1961). The velocity of compressional waves in rocks to 10 kilobars, Part 2, *J. Geophys. Res.* **66**, 2199–2224.
- Burridge, R. (1976). *Some Mathematical Topics in Seismology*, Courant Institute of Mathematical Sciences, New York University, New York.
- Fang, Y., and G. Müller (1996). Attenuation operators and complex wave velocities for scattering in random media, *Pure Appl. Geophys.* **148**, 269–285.
- Fehler, M., H. Sato, and L.-J. Huang (2000). Envelope broadening of outgoing waves in 2D random media: a comparison between the Markov approximation and numerical simulations, *Bull. Seism. Soc. Am.* **90**, 914–928.
- Frankel, A., and R. Clayton (1986). Finite difference simulation of seismic scattering: implications for the propagation of short-period seismic waves in the crust and models in crustal heterogeneity, *J. Geophys. Res.* **91**, 6465–6489.
- Frenje, L., and C. Juhlin (2000). Scattering attenuation: 2-D and 3-D finite difference simulations vs. theory, *J. Appl. Geophys.* **44**, 33–46.
- Furumura, M., B. L. N. Kennett, and T. Furumura (1999). Seismic wavefield calculation for laterally heterogeneous earth models. II. The influence of upper mantle heterogeneity, *Geophys. J. Int.* **139**, 623–644.
- Hong, T.-K., and B. L. N. Kennett (2002a). A wavelet-based method for simulation of two-dimensional elastic wave propagation, *Geophys. J. Int.* **150**, 610–638.
- Hong, T.-K., and B. L. N. Kennett (2002b). On a wavelet-based method for the numerical simulation of wave propagation, *J. Comput. Phys.* **183**, 577–622.
- Hoshida, M. (2000). Large fluctuation of wave amplitude produced by small fluctuation of velocity structure, *Phys. Earth Planet. Inter.* **120**, 201–217.
- Hudson, J. A., and J. R. Heritage (1981). The use of the Born approximation in seismic scattering problems, *Geophys. J. R. Astr. Soc.* **66**, 221–240.
- Jannaud, L. R., P. M. Adler, and C. G. Jacquini (1991). Frequency dependence of the Q factor in random media, *J. Geophys. Res.* **96**, 18,233–18,243.
- Kanasewich, E. R. (1981). *Time Sequence Analysis in Geophysics*, Third Ed., The University of Alberta Press, Alberta, Canada.
- Kawahara, J. (2002). Cutoff scattering angles for random acoustic media, *J. Geophys. Res.* **107** (B1), 10.1029/2001JB000429.
- Kennett, B. L. N. (1972). Seismic waves in laterally inhomogeneous media, *Geophys. J. R. Astr. Soc.* **27**, 301–336.
- Kennett, B. L. N. (1983). *Seismic Wave Propagation in Stratified Media*, Cambridge University Press, Cambridge.
- Kennett, B. L. N. (2001). *The Seismic Wavefield* Vol. 1, Cambridge University Press, Cambridge.
- Kennett, B. L. N., E. R. Engdahl, and R. Buland (1995). Constraints on seismic velocities in the earth from travel times, *Geophys. J. Int.* **122**, 108–124.
- Klimeš, L. (2002). Correlation functions of random media, *Pure Appl. Geophys.* **159**, 1811–1831.
- Komatitsch, D., and J.-P. Vilotte (1998). The spectral element method: an efficient tool to simulate the seismic response of 2D and 3D geological structures, *Bull. Seism. Soc. Am.* **88**, 368–392.
- Mai, P. M., and G. C. Beroza (2002). A spatial random-field model to

- characterize complexity in earthquake slip, *J. Geophys. Res.* **107** (B11), 10.1029/2001JB000588.
- Nolet, G., S. P. Grand, and B. L. N. Kennett (1994). Seismic heterogeneity in the upper mantle, *J. Geophys. Res.* **99**, 23,753–23,766.
- Roth, M., and M. Korn (1993). Single scattering theory versus numerical modelling in 2-D random media, *Geophys. J. Int.* **112**, 124–140.
- Sato, H. (1982). Amplitude attenuation of impulsive waves in random media based on travel time corrected mean wave formalism, *J. Acoust. Soc. Am.* **71**, 559–564.
- Sato, H. (1984). Attenuation and envelope formation of three-component seismograms of small local earthquakes in randomly inhomogeneous lithosphere, *J. Geophys. Res.* **89**, 1221–1241.
- Sato, H., and M. Fehler (1998). *Seismic Wave Propagation and Scattering in the Heterogeneous Earth*, Springer-Verlag, New York.
- Shapiro, N. M., K. B. Olsen, and S. K. Singh (2000). Wave-guide effects in subduction zones: evidence from three-dimensional modeling, *Geophys. Res. Lett.* **27**, 433–436.
- Shiomi, K., H. Sato, and M. Ohtake (1997). Broadband power-bin spectra of well-log data in Japan, *Geophys. J. Int.* **130**, 57–64.
- Wu, R. S. (1982). Attenuation of short period seismic waves due to scattering, *Geophys. Res. Lett.* **9**, 9–12.
- Wu, R. S. (1989). The perturbation method in elastic wave scattering, *Pure Appl. Geophys.* **131**, 605–637.
- Wu, R. S., and K. Aki (1985). Elastic wave scattering by a random medium and the small-scale inhomogeneities in the lithosphere, *J. Geophys. Res.* **90**, 10,261–10,273.
- Wu, R. S., S. Jin, and X.-B. Xie (2000). Seismic wave propagation and scattering in heterogeneous crustal waveguides using screen propagation: I. SH waves, *Bull. Seism. Soc. Am.* **90**, 401–413.
- Wu, R. S., Z. Xu, and X.-P. Li (1994). Heterogeneity spectrum and scale-anisotropy in the upper crust revealed by the German continental deep-drilling (KTB) holes, *Geophys. Res. Lett.* **21**, 911–914.
- Yomogida, K., and R. Benites (1995). Relation between direct wave Q and Coda Q: a numerical approach, *Geophys. J. Int.* **123**, 471–483.

Appendix A

Procedure for Ensemble Average

We consider the ensemble average of the velocity fluctuations in equations (26):

$$\begin{aligned}
 \langle |u_r^{PP}|^2 \rangle &= \frac{k^3}{8\pi|\mathbf{x}|} [C_r(\theta)]^2 \\
 &\times \int_S \int_S \langle \xi(\mathbf{x}')\xi(\mathbf{y}') \rangle \exp [ik\{\mathbf{e}_z \cdot (\mathbf{x}' - \mathbf{y}') - \mathbf{n} \\
 &\quad \cdot (\mathbf{x}' - \mathbf{y}')\}] dS(\mathbf{x}')dS(\mathbf{y}'), \\
 \langle |u_t^{PS}|^2 \rangle &= \frac{k^3\gamma^3}{8\pi|\mathbf{x}|} [C_t(\theta)]^2 \\
 &\times \int_S \int_S \langle \xi(\mathbf{x}')\xi(\mathbf{y}') \rangle \exp [ik\{\mathbf{e}_z \cdot (\mathbf{x}' - \mathbf{y}') - \gamma\mathbf{n} \\
 &\quad \cdot (\mathbf{x}' - \mathbf{y}')\}] dS(\mathbf{x}')dS(\mathbf{y}'), \quad (\text{A1})
 \end{aligned}$$

where \mathbf{e}_z is the unit vector for the z -axis direction and \mathbf{n} is the unit vector for \mathbf{x} direction in equations (16) and (17). We make a change of variables from \mathbf{x}' and \mathbf{y}' to \mathbf{p} (center-of-mass coordinate variable) and \mathbf{q} (relative coordinate variable) by

$$\mathbf{p} = (\mathbf{x}' + \mathbf{y}')/2, \quad \mathbf{q} = \mathbf{x}' - \mathbf{y}'. \quad (\text{A2})$$

Also, we introduce difference vectors \mathbf{E}_r and \mathbf{E}_t to simplify the integrals for the radial and tangential ensemble average:

$$\begin{aligned}
 \mathbf{E}_r &= \mathbf{e}_z - \mathbf{n} = (-\sin\theta, 1 - \cos\theta), \quad |\mathbf{E}_r| = 2 \sin(\theta/2), \\
 \mathbf{E}_t &= \mathbf{e}_z - \gamma\mathbf{n} = (-\gamma\sin\theta, 1 - \gamma\cos\theta), \\
 |\mathbf{E}_t| &= \sqrt{1 + \gamma^2 - 2\gamma\cos\theta}. \quad (\text{A3})
 \end{aligned}$$

When we consider the integrals in equation (A1) with variables \mathbf{p} and \mathbf{q} , the integration over \mathbf{p} yields the area S and can simplify the resulting equations using \mathbf{E}_r and \mathbf{E}_t to the form

$$\begin{aligned}
 \langle |u_r^{PP}|^2 \rangle &= \frac{Sk^3}{8\pi|\mathbf{x}|} [C_r(\theta)]^2 \int_S \langle \xi(\mathbf{x}')\xi(\mathbf{y}') \rangle \exp [ik\mathbf{E}_r \cdot \mathbf{q}] dS(\mathbf{q}), \\
 \langle |u_t^{PS}|^2 \rangle &= \frac{Sk^3\gamma^3}{8\pi|\mathbf{x}|} [C_t(\theta)]^2 \int_S \langle \xi(\mathbf{x}')\xi(\mathbf{y}') \rangle \exp [ik\mathbf{E}_t \cdot \mathbf{q}] dS(\mathbf{q}). \quad (\text{A4})
 \end{aligned}$$

The integration over \mathbf{q} is simple in a polar coordinate system (r' , ϕ'):

$$r' = |\mathbf{q}|, \quad dS(\mathbf{q}) = r' dr' d\phi', \quad (\text{A5})$$

and the ensemble of fluctuation $\langle \xi(\mathbf{x}')\xi(\mathbf{y}') \rangle$ can be represented by the autocorrelation function (ACF) $N(r')$ for the stochastic media. Therefore, equation (A4) can be written using equations (A3) and (A5) as

$$\begin{aligned}
 \langle |u_r^{PP}|^2 \rangle &= \frac{Sk^3}{8\pi|\mathbf{x}|} [C_r(\theta)]^2 \int_{r=0}^{r=\infty} \int_{\phi'=-\pi}^{\phi'=\pi} N(r') \exp \left[i2kr' \sin\left(\frac{\theta}{2}\right) \cos\phi' \right] r' dr' d\phi', \\
 \langle |u_t^{PS}|^2 \rangle &= \frac{Sk^3\gamma^3}{8\pi|\mathbf{x}|} [C_t(\theta)]^2 \int_{r=0}^{r=\infty} \int_{\phi'=-\pi}^{\phi'=\pi} N(r') \exp \left[ikr' \sqrt{1 + \gamma^2 - 2\gamma\cos\theta} \cos\phi' \right] \\
 &\quad r' dr' d\phi'. \quad (\text{A6})
 \end{aligned}$$

We can express the power spectral density for the stochastic medium in terms of $N(\mathbf{r})$ through a 2D Fourier transform, which can be recast as a Hankel transform using the representation of the zeroth order Bessel function ($J_0(x)$) as angular integral over the exponential function (cf., Frankel and Clayton, 1986)

$$\int_{-\pi}^{\pi} \exp[ix\cos\phi'] d\phi' = 2\pi J_0(x), \quad (\text{A7})$$

$$\mathcal{P}(k) = 2\pi \int_0^{\infty} N(r') r' J_0(kr') dr'. \quad (\text{A8})$$

With these relations we can rewrite equation (A6) as

$$\begin{aligned} \langle |u_r^{PP}|^2 \rangle &= \frac{k^3 S}{8\pi |x|} [C_r(\theta)]^2 \cdot P \left[2k \sin \frac{\theta}{2} \right], \\ \langle |u_t^{PS}|^2 \rangle &= \frac{k^3 \gamma^3 S}{8\pi |x|} [C_t(\theta)]^2 \cdot P \left[k \sqrt{1 + \gamma^2 - 2\gamma \cos \theta} \right], \end{aligned} \quad (\text{A9})$$

where $P(k)$ is the power spectral density function (PSDF), spectrum of ACF $N(r)$.

Research School of Earth Sciences
 Institute of Advanced Studies
 The Australian National University
 Canberra ACT 0200, Australia.
tkhong@rse.s.anu.edu.au
brian@rse.s.anu.edu.au
 (T.-K.H., B.L.N.K.)

Manuscript received 26 February 2002.